CONSTRAINED BUNDLE ADJUSTMENT APPLIED TO WING 3D RECONSTRUCTION WITH MECHANICAL LIMITATIONS

Quentin Demoulin[1,2]*, François Lefebvre-Albaret*[1]*, Adrian Basarab*[3]*, Denis Kouamé*[3]*, and Jean-Yves Tourneret*[2]

[1]*Airbus, 316 route de Bayonne, 31060 Toulouse, France*
[2]*IRIT/ENSEEIHT/Tésa, University of Toulouse, 31071 Toulouse, France*
[3]*IRIT UMR CNRS 5505, University of Toulouse, Université Paul Sabatier, CNRS, France*

ABSTRACT

Aircraft certification procedures require the estimation of wing deformation, which is a very challenging problem in photogrammetry applications. Indeed, in real flight conditions with varying environment, 3D reconstruction is strongly degraded. To cope with this issue, we propose to introduce prior knowledge about the wing mechanical limits in the photogrammetry reconstruction method. These mechanical limits are expressed as appropriate regularizations that are included into the classical bundle adjustment step. The proposed approach is evaluated using data acquired on a real aircraft yielding promising results.

***Index Terms*—** Bundle adjustment, optimization under constraints, wing deformations, mechanical limits.

1. INTRODUCTION

In aircraft certification procedures, estimating the 3D deformations of wings is necessary to evaluate and improve theoretical models of the aircraft behaviour under various conditions (aircraft weight, speed, angle of attack, etc.). In order to estimate these deformations during flight, we propose a new multiple-view photogrammetry approach based on Bundle Adjustment (BA) using cameras installed in the aircraft. BA is a classical method for estimating jointly a 3D scene and camera positions [1, p. 434]. First introduced for photogrammetry reconstructions, it has also been widely used and improved in robotics and computer applications, through structure from motion (SfM) [2, 3] and full simultaneous localization and mapping (SLAM) [4] methods. BA is an iterative method, which seeks to minimize a non-linear and non convex objective function. Consequently, its convergence to a global minimum of the cost function is not guaranteed and its strong dependence to initial conditions can be a critical issue.

For the reasons mentioned above, 3D wing reconstruction in flight is a very challenging problem in photogrammetry. On the one hand, camera positions are subject to strong installation constraints. The only possible camera locations are on the rear vertical stabilizer of the aircraft and on the aircraft windows. In such configuration, the end of the wing is viewed under very low angle, which will strongly impact the accuracy of point detection in the images. Moreover, the distance between cameras is also limited to guaranty overlapping in views of the wing (about 15m distance for a 30m long wing). On the other hand, we must face highly varying environment, with luminosity changes, presence of possible reflections or shadows, vibrations and deformations of the entire aircraft. In this context, the classical BA method generally suffers from observation imprecisions leading to many outliers.

To improve the performance of the classical BA method, different constrained optimization strategies have been proposed over the years, introducing prior knowledge about the systems or scenes to reconstruct. In [2, 5, 6], prior knowledge about the camera positions constructed from Global Positioning System (GPS) or Inertial Measurement Unit (IMU) data are introduced in the BA as constraints for the camera parameters. Similarly coplanarity between neighbours or constraints on their positions through prior knowledge of a Digital Terrain Model (DTM) of the scene can be introduced in the BA method [7, 8]. Note that GPS and DTM were used jointly as priors to improve SLAM accuracy and robustness in [9]. Finally, we would like to mention the use of prior knowledge about 3D structure models, which were used in model-assisted BA to enforce reconstructed 3D points to be close to a reference model [10], [11].

In order to improve BA for wing deformation estimation, the structure model cannot be used directly since it depends on the model to be evaluated. The main contribution of this paper is to investigate some prior knowledge resulting from wing mechanical limits, beyond which the wing would break. To this aim, we introduce an appropriate regularization in the BA cost function [12, p. 564] constraining the 3D points to respect these mechanical limits.

The remainder of the paper is organized as follows. Section 2 recalls the principle of BA for 3D wing reconstruction. Section 3 introduces the proposed mechanical constraints that are used to define a new BA cost function defined in Section 4. Experimental results are presented in Section 5. Conclusions and perspectives are reported in Section VI.

The authors would like to thank Airbus for funding and support.

2. BUNDLE ADJUSTMENT

BA is a common method, used in photogrammetry with more than 2 views, to recover 3D-point coordinates and camera parameters from 2D observations. Denote as $\boldsymbol{\alpha}_j = (\phi^j, \theta^j, \psi^j, \boldsymbol{t}_j)^T$ the parameter vector of the camera j, where ϕ^j, θ^j, ψ^j are the rotation angles and $(\boldsymbol{t}_j)$ is the 3×1 translation vectors of the cameras. Given a set of M cameras and N 3D-points denoted as $\boldsymbol{X}^i$ for $i = 1, ..., N$, the algorithm seeks to minimize the distance between the projections of $\boldsymbol{X}^i$ on camera j (for $j = 1, \ldots, M$), denoted as $\hat{\boldsymbol{x}}(\boldsymbol{\alpha}_j, \boldsymbol{X}^i)$ and the corresponding observed 2D points $(\boldsymbol{x}_j^i)$ from camera images:

$$\underset{\boldsymbol{\alpha}_j, \boldsymbol{X}^i}{\arg\min} \sum_{i,j} \left[\boldsymbol{x}_j^i - \hat{\boldsymbol{x}}(\boldsymbol{\alpha}_j, \boldsymbol{X}^i)\right]^2, \tag{1}$$

where

$$\hat{\boldsymbol{x}}(\boldsymbol{\alpha}_j, \boldsymbol{X}^i) = \frac{1}{w_j^i} \boldsymbol{K}_j \boldsymbol{l}_j^i, \tag{2}$$

where $\boldsymbol{K}_j$ is the 2×3 matrix of the intrinsic camera parameters, considered as known after system calibration, and

$$\boldsymbol{l}_j^i = (u_j^i, v_j^i, w_j^i)^T = \left[\boldsymbol{R}_j^T, -\boldsymbol{R}_j^T \boldsymbol{t}_j\right] \boldsymbol{X}^i \tag{3}$$

with $\boldsymbol{R}_j$ the rotation matrix formed using Euler angles as

$$\boldsymbol{R}_j = \begin{bmatrix} 1 & 0 & 0 \\ 0 & \cos(\theta_j) & -\sin(\theta_j) \\ 0 & \sin(\theta_j) & \cos(\theta_j) \end{bmatrix} \times \begin{bmatrix} \cos(\phi_j) & 0 & \sin(\phi_j) \\ 1 & 0 & 0 \\ -\sin(\phi_j) & 0 & \cos(\phi_j) \end{bmatrix} \times \begin{bmatrix} \cos(\psi_j) & -\sin(\psi_j) & 0 \\ \sin(\psi_j) & \cos(\psi_j) & 0 \\ 0 & 0 & 1 \end{bmatrix}.$$

The estimation problem (1) is highly non-convex and thus needs to be solved with efficient optimization methods. One can think of using iterative methods such as Gauss-Newton or Levenberg Marquardt (see [8] or [1, p. 597]). In both methods, the iterative steps from the initial guess to the optimum parameter vector is guided by the Hessian matrix, which is approximated as $\boldsymbol{J}^T\boldsymbol{J}$, where $\boldsymbol{J}$ is the Jacobian matrix.

An interesting property of the BA method is that the Jacobian matrix (used for the different minimization steps) is sparse, which allows the optimization to be fastened significantly. Indeed, each projected point depends only on the corresponding 3D point and camera, leading to:

$$\frac{\partial(\boldsymbol{x}_j^p - \hat{\boldsymbol{x}}(\boldsymbol{\alpha}_j, \boldsymbol{X}^p))^2}{\partial \boldsymbol{X}^q} = 0, \forall p \neq q, \forall j \in \{1, ..., M\} \tag{4}$$

$$\frac{\partial(\boldsymbol{x}_p^i - \hat{\boldsymbol{x}}(\boldsymbol{\alpha}_p, \boldsymbol{X}^i))^2}{\partial \boldsymbol{\alpha}_q} = 0, \forall p \neq q, \forall i \in \{1, ..., N\}. \tag{5}$$

Moreover, all points are not necessarily seen by all cameras, resulting in additional zero lines in the Jacobian matrix. The final shape of the Jacobian is displayed in Fig. 1, where the white elements denote the only non-zero entries of the matrix.

3. MECHANICAL CONSTRAINTS

In the specific case of wing deformations, one have access to the Finite Element Models (FEM) of the wing, which allows to calculate 3D wing shapes for all possible flight configurations. These models can represent regular flight conditions (which can not be used, as they are to be validated), but also limit conditions corresponding to the limits of the wing materials. The approach considered in this work consists in defining a constrained BA algorithm, exploiting these maximum and minimum deformation limits that can be supported by the aircraft. More precisely, these limits correspond to the extreme cases where the wing would break, which we assume is not possible during the tests. These extreme cases lead to an envelop of wing deformations, which will be used in the estimation algorithm.

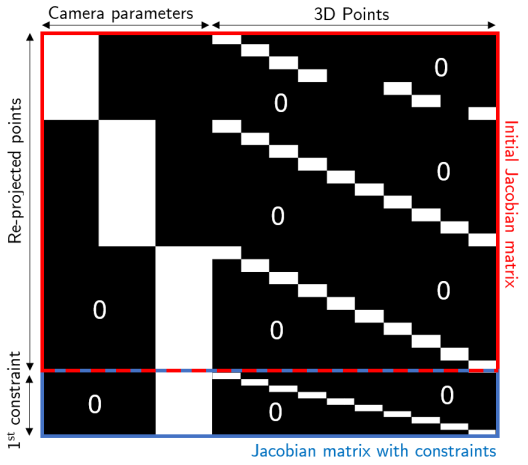

Fig. 1. Example of sparse bundle adjustment Jacobian matrix for 3 cameras and 10 points. The last rows represents the simple constraint used in Section 5.

Denoting as $\boldsymbol{X}^i = (x^i, y^i, z^i)$ the ith deformation point, and using axes shown in Fig. 2, several limits can be taken into account. These limits include

i. Volume constraints: each point has a specific volume limit (sphere, ellipsoid, or some volume defined according to the FEM data).

ii. Bending constraints: $\forall i, \exists(b_{\min}^i, b_{\max}^i)$, such that the bending $\frac{\partial^2 z^i}{\partial y^2}$ ranges in $[b_{\min}^i, b_{\max}^i]$,

iii. Torsion constraints: $\forall i, \exists(t_{\min}^i, t_{\max}^i)$, such that the torsion $\frac{\partial^2 z^i}{\partial x \partial y}$ ranges in $[t_{\min}^i, t_{\max}^i]$,

iv. Relative elongation constraint: $\forall i, \exists \epsilon^i$, such that

$$\frac{d(\boldsymbol{X}^i, \boldsymbol{X}^{i-1}) - d_0(\boldsymbol{X}^i, \boldsymbol{X}^{i-1})}{d_0(\boldsymbol{X}^i, \boldsymbol{X}^{i-1})} < \epsilon^i \tag{6}$$

where $d(\boldsymbol{X}^i, \boldsymbol{X}^{i-1})$ is the Euclidean distance between points $\boldsymbol{X}^i$ and $\boldsymbol{X}^{i-1}$ in the (x, y) plane, and $d_0(\boldsymbol{X}^i, \boldsymbol{X}^{i-1})$ is the initial distance before deformation.

In addition to the constraints mentioned before, we propose to detect points of interest located on the lines naturally present on the wing (represented in Fig. 2 as green lines). Assuming that the constraints are locally valid, we can specify them numerically on a finite set of nodes in the (x, y) plane. As an illustration, consider the node $\boldsymbol{X}^i = (x_i, y_i, z_i)^T$ and its neighbourhood $(\boldsymbol{X}^{i-2}, \ldots, \boldsymbol{X}^{i+2}, \boldsymbol{X}'^{i-2}, \ldots, \boldsymbol{X}'^{i+2})$, as displayed in Fig. 2. The possible constraints for $\boldsymbol{X}^i$ are:

i. Volume constraint: for the simple case of a spherical volume with radius r^i, the constraint can be written:

$$\left\|\boldsymbol{X}^i - \boldsymbol{X}^i_{\text{init}}\right\| \leq r^i, \tag{7}$$

with $\boldsymbol{X}^i_{\text{init}}$ the initial position of the point i before deformation, and $\|.\|$ an appropriate norm (the ℓ_2 norm in this paper).

ii. Bending constraints: $\forall i, \exists(b_{\min}, b_{\max})$, such that

$$b^i_{\min} < \frac{z_{i+1} - 2z_i + z_{i-1}}{(y_{i+1} - y_i)^2} < b^i_{\max}. \tag{8}$$

iii. Torsion constraints: The two nodes $\boldsymbol{X}^i$ and $\boldsymbol{X}'^i$ are constrained by the adjacent nodes $\boldsymbol{X}^{i-1}$ and $\boldsymbol{X}'^{i-1}$, leading to $\forall i, \exists(t^i_{\min}, t^i_{\max})$ such that

$$t^i_{\min} < \frac{z'_i - z'_{i-1} - z_i + z_{i-1}}{4(x'_i - x_i)(y_i - y_{i-1})} < t^i_{\max}. \tag{9}$$

iv. The elongation constraint remains unchanged.

4. CONSTRAINED BUNDLE ADJUSTMENT

Before applying the constraints on our set of estimated 3D points, a registration phase is necessary. Indeed, in this application, constraints are defined in the aircraft coordinate system, while camera and point positions are estimated in a moving coordinate system, due to camera motions during the flight. To overcome this issue, we first find the transfer matrix $\boldsymbol{P}$ from the aircraft coordinate system to the rear camera system, using reference points visible only from the rear view. Then, using the estimated parameters $\boldsymbol{\alpha}_k$ from the same camera, the registered points $\tilde{\boldsymbol{X}}^i$ can be calculated as follows:

$$\tilde{\boldsymbol{X}}^i = \boldsymbol{P}\left[\boldsymbol{R}_k^T, -\boldsymbol{R}_k^T \boldsymbol{t}_k\right] \boldsymbol{X}^i. \tag{10}$$

After the registration phase, the constraints defined in Section 3 can be transformed into regularization terms penalizing the cost function (1) [12, p. 564]. This allows us to define the following regularized optimization problem:

$$\underset{\boldsymbol{\alpha_j}, \boldsymbol{X}^i}{\arg\min} \sum_{i,j} \left[\boldsymbol{x}^i_j - \hat{\boldsymbol{x}}(\boldsymbol{\alpha}_j, \boldsymbol{X}^i)\right]^2 + \mu \sum_i \left[g^+(\boldsymbol{\alpha}_k, \boldsymbol{X}^i)\right]^2, \tag{11}$$

where μ is a positive penalty parameter (to be adjusted by the user), and $g^+(\boldsymbol{\alpha}_k, \boldsymbol{X}^i) = \max(0, g(\boldsymbol{\alpha}_k, \boldsymbol{X}^i))$, with g the considered constraint (which can be extended to several constraints by including several regularizations). The experimentation described in this paper corresponds to a simple constraint, stating that 3D points have limited displacements in the (x, y) plane, leading to the following constraints:

$$g(\boldsymbol{\alpha}_k, \boldsymbol{X}^i) = \sqrt{(\tilde{x}^i - x^i_{\text{init}})^2 + (\tilde{y}^i - y^i_{\text{init}})^2} - a^i \tag{12}$$

where a^i is the maximum radius at point $\boldsymbol{X}^i$.

Note that when the constraint is respected, the penalty term equals zero. Moreover, we choose the *Courant-Beltrami* penalty function [12, p. 566] with a quadratic term, in order to ensure that the cost function is differentiable when $g(\boldsymbol{\alpha}_k, \boldsymbol{X}^i) = 0$. As a a result, classical optimization methods based on the Jacobian matrix can be applied to solve (11). Finally, it is interesting to note that the Jacobian matrix for the cost function in (11) is still sparse (as shown in Fig. 1) since the constrains are applied to specific points and their neighbours and depend only on the rear camera parameters. This sparsity of the Jacobian matrix induces a reduced computational cost for the final constrained optimization algorithm.

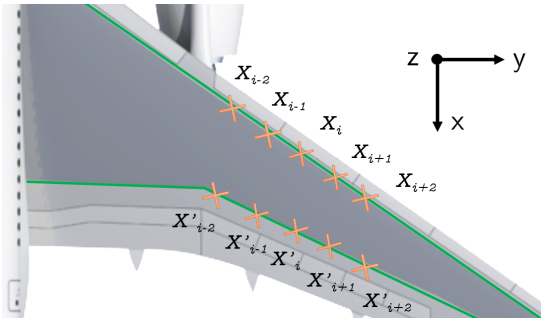

Fig. 2. Node illustration on the aircraft wing.

5. EXPERIMENTAL RESULTS

The proposed method was evaluated on a set of real images acquired on an Airbus A350-900 located on ground. The test was conducted in order to reproduce in-flight vibrations. Four 4K cameras were placed on the aircraft window and a drone was used to simulate the rear camera. Different focal lengths were used to ensure a similar accuracy in far and close parts of the wing. Some examples of views acquired with these cameras are displayed in Fig. 3. Red tape markers were installed on the two black lines of the wing at approximately every 30 cm to clearly identify nodes on which we will apply the deformation constraints. Some cross targets were also installed to guarantee a good detection of these points. To ensure a good initialization of the camera parameters and point positions, we scanned the wing using a drone and the software Agisoft Metashape [13]. Finally, the wing was shaken manually at its tip to make it vibrate. Using a scale board placed at the end of the wing, we estimated a bending of about 5 cm. As expected, moving reflections appeared on the wing for several views (visible on camera 3 in Fig. 3), preventing good graduation detections in images. Furthermore, the graduations viewed under the lowest angles were detected with a reduced accuracy.

The proposed new algorithm was implemented on Python and compared to solution without constraints. The optimization was performed for both algorithms using the Least-squares method implemented in the Scipy library [14] (function "scipy.optimize.least_squares").

After running our method on a set of 30 representative images of the moving wing, we extracted the camera and point parameters estimated with and without the constraint (respectively denoted as "CBA" and "BA"). The radius a^i defined in (12) was fixed by experts to 5 cm, which is in good agreement with typical measurements from stress gauges in flight. Fig. 4 shows that using the constrained algorithm improves

(a) Camera 1 (b) Rear camera (c) Camera 3

Fig. 3. Examples of recorded views resulting from a the test on ground with an Airbus A350-900.

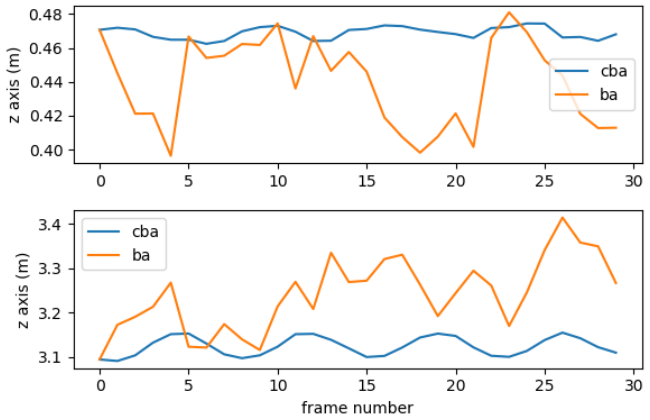

Fig. 4. Bending results at the middle of the wing (top) and at wing tip (bottom).

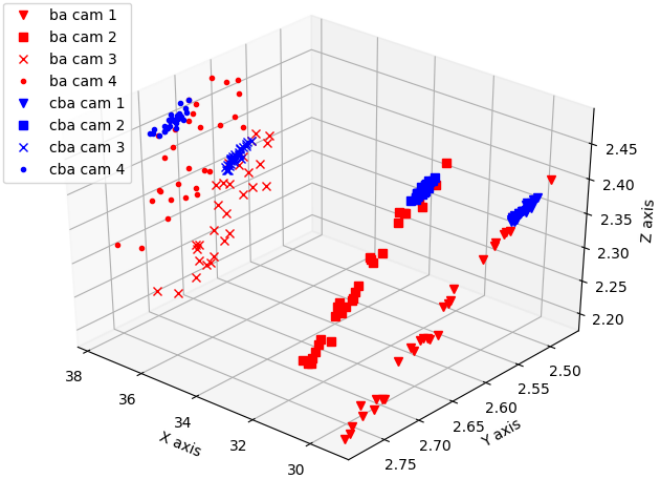

Fig. 5. Estimated motions (in meters) of the 4 cameras located on the aircraft windows versus time.

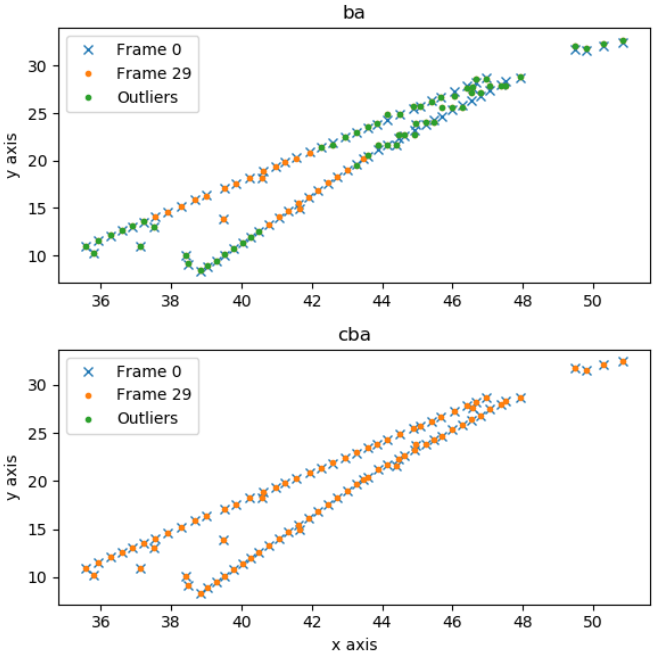

Fig. 6. Point reconstructions in the (x, y) plane for the first and last frames. (top) without the constraint, (bottom) with the constraint. Some outliers do not respecting the constraints can be observed in the last frame.

the estimation results significantly. The point displacements obtained using CBA along the z axis are much more coherent than the unconstrained points. Indeed, these CBA points have a sinusoidal shape with an amplitude close to 5cm amplitude at the wing tip, and with an amplitude less than 1cm in the middle of the wing (corresponding to what was measured using the scale board). In addition, Fig. 5 shows that the CBA algorithm also provides better camera position estimates. Indeed, since the test was performed on ground, camera were fixed with negligible motions. Finally, the point positions estimated using the CBA algorithm seem to be tracked correctly, as illustrated in Fig. 6. This last figure also confirms that the constraint was correctly applied, with all points located close to their initial positions in the (x, y) plan.

6. CONCLUSIONS

This paper presented a new method to improve photogrammetry-based 3D estimation of wing deformations in real flight conditions. The main idea was to introduce mechanical constraints as regularizations in the classical bundle adjustment cost function. A realistic experimentation conducted on images acquired on ground showed the interest of using constrained bundle adjustment, with a simple displacement constraint for the 3D points. Future work will focus on the application, in flight, of other constraints resulting from finite element models (e.g., see [15]). Another line of research would be to investigate weighted bundle adjustment to mitigate the inaccuracy of some observations.

7. REFERENCES

[1] R. Hartley and A. Zisserman, *Multiple View Geometry in Computer Vision*, Cambridge University Press, New York, NY, USA, 2004.

[2] D. Larnaout, V. Gay-Bellile, S. Bourgeois, and M. Dhome, "Vehicle 6-DoF localization based on SLAM constrained by GPS and digital elevation model information," in *Proc. Int. Conf Image Process. (ICIP)*, Melbourne, Australia, Sep. 2013.

[3] A. P. Bustos, T.-J. Chin, A. Eriksson, and I. Reid, "Visual SLAM: Why bundle adjust?," in *Proc. Int. Conf. on Robotics and Automation (ICRA)*, Montréal, Canada, May. 2019.

[4] V. Indelman, R. Roberts, and F. Dellaert, "Incremental light bundle adjustment for structure from motion and robotics," *Robotics and Autonomous Systems*, vol. 70, pp. 63–82, Aug. 2015.

[5] B. Heiner and C. N. Taylor, "Creation of geo-referenced mosaics from MAV video and telemetry using constrained optimization bundle adjustment," in *Proc. Int. Conf. on Intelligent Robots and Systems*, St Louis, St Louis, USA, Oct. 2009.

[6] M. Lhuillier, "Incremental fusion of structure-from-motion and GPS using constrained bundle adjustments," *IEEE Trans. Pattern Anal. Mach. Intell.*, vol. 34, no. 12, pp. 2489–2495, Dec. 2012.

[7] Y. Zhang, K. Hu, and R. Huang, "Bundle adjustment with additional constraints applied to imagery of the dunhuang wall paintings," *ISPRS Journal of Photogrammetry and Remote Sensing*, vol. 72, pp. 113–120, Aug. 2012.

[8] G. Briskin, A. Geva, E. Rivlin, and H. Rotstein, "Estimating pose and motion using bundle adjustment and digital elevation model constraints," *IEEE Trans. Aerosp. Electron. Syst.*, vol. 53, no. 4, pp. 1614–1624, Aug. 2017.

[9] D. Larnaout, S. Bourgeois, V. Gay-Bellile, and M. Dhome, "Towards bundle adjustment with GIS constraints for online geo-localization of a vehicle in urban center," in *Proc. Int. Conf. on 3D Imaging, Modeling, Processing, Visualization & Transmission (3DIMPVT)*, Zurich, Switzerland, Oct. 2012.

[10] P. Fua, "Using model-driven bundle-adjustment to model heads from raw video sequences," in *Proc. Int. Conf. Comput. Vis. (ICCV)*, Kerkyra, Greece, Sep. 1999.

[11] P. Ozog, M. Johnson-Roberson, and R. M. Eustice, "Mapping underwater ship hulls using a model-assisted bundle adjustment framework," *Robotics and Autonomous Systems*, vol. 87, pp. 329–347, Jan. 2017.

[12] E. K. P. Chong and S. H. Zak, *An Introduction to Optimization*, Wiley, 2013.

[13] Agisoft LLC, St. Petersburg, Russia, *Agisoft Metashape User Manual: Professional Edition, Version 1.6*, 2020, available at: https://www.agisoft.com/downloads/user-manuals/.

[14] P. Virtanen and al., "SciPy 1.0: Fundamental Algorithms for Scientific Computing in Python," *Nature Methods*, 2020.

[15] Q. Demoulin, F. Lefebvre-Albaret, A. Basarab, D. Kouamé, and J. Y. Tourneret, "Wing 3D reconstruction by constraining the bundle adjustment with mechanical limitations," in *Proc. 28th European Signal Process. Conf. (EUSIPCO)*, Amsterdam, Netherlands, Jan. 2021.